Experimental Eye Research 224 (2022) 109266

Contents lists available at ScienceDirect

Experimental Eye Research

journal homepage: www.elsevier.com/locate/yexer

Research article

Orientation and depth dependent mechanical properties of the porcine cornea: Experiments and parameter identification

Malavika H. Nambiar [a], Layko Liechti [a], Fabian Müller [b], Werner Bernau [b], Harald Studer [c], Abhijit S. Roy [d], Theo G. Seiler [e,f,g], Philippe Büchler [a,*]

[a] ARTORG Center for Biomedical Engineering Research, University of Bern, Freiburgstrasse 3, 3010, Bern, Switzerland
[b] Ziemer Ophthalmic Systems AG, Allmendstrasse 11, 2562, Port, Switzerland
[c] Optimo Medical, Robert-Walser-Platz 7, 2503, Biel, Switzerland
[d] Narayana Nethralaya Eye Clinic, Bengaluru, Karnataka, 560010, India
[e] IROC AG, Institut für Refraktive und Ophthalmo-Chirurgie, Stockerstrasse 37, 8002, Zürich, Switzerland
[f] Universitätsklinik für Augenheilkunde, Inselspital Bern, Freiburgstrasse 15, 3010, Bern, Switzerland
[g] Universitätsklinikum Düsseldorf, Germany

ARTICLE INFO

Keywords:
Porcine cornea
Biomechanics
Material characterization
Uniaxial test
Finite element methods

ABSTRACT

The porcine cornea is a standard animal model in ophthalmic research, making its biomechanical characterization and modeling important to develop novel treatments such as crosslinking and refractive surgeries. In this study, we present a numerical model of the porcine cornea based on experimental measurements that captures both the depth dependence and orientation dependence of the mechanical response. The mechanical parameters of the established anisotropic hyperelastic material models of Gasser, Holzapfel and Ogden (HGO) and Markert were determined using tensile tests. Corneas were cut with a femtosecond laser in the anterior (100 μm), central (350 μm), and posterior (600 μm) regions into nasal-temporal, superior-inferior, and diagonal strips of 150 μm thickness. These uniformly thick strips were tested at a low speed using a single-axis testing machine. The results showed that the corneal mechanical properties remained constant in the anterior half of the cornea regardless of orientation, but that the material softened in the posterior layer. These results are consistent with the circular orientation of collagen observed in porcine corneas using X-ray scattering. In addition, the parameters obtained for the HGO model were able to reproduce the published inflation tests, indicating that it is suitable for simulating the mechanical response of the entire cornea. Such a model constitutes the basis for in silico platforms to develop new ophthalmic treatments. In this way, researchers can match their experimental surrogate porcine model with a numerical counterpart and validate the prediction of their algorithms in a complete and accessible environment.

1. Introduction

The first studies in ophthalmology using the porcine eyeball date back to the late 1850s (Carter, 1872; Vail, 1956). Whether for the development of new instruments, surgical techniques, or grafts, the anatomical similarity of the porcine eye to the human eye and its availability have proven indispensable to researchers in ophthalmology, particularly for the anterior segment of the eye (Sanchez et al., 2011; Zeiss, 2013). Understanding corneal biomechanics is critical for any procedure that aims to change the shape of the cornea such as refractive interventions, or its stiffness, such as in crosslinking (Roberts, 2016). Because porcine corneas are commonly used to develop procedures for pathologies such as keratoconus, their accurate biomechanical characterization is critical.

Various methods have been used to quantify the biomechanics of porcine corneas, including inflation (Boschetti et al., 2012), shear (Hatami-marbini, 2014) (Søndergaard et al., 2013), indentation (Ahearne et al., 2007), air puff (Bekesi et al., 2016) or tensile testing (Boschetti et al., 2012; Du et al., 2017; Elsheikh, A. et al., 2008; Elsheikh et al., 2011; Elsheikh and Alhasso, 2009; Kampmeier et al., 2000;

* Corresponding author. Freiburgstrasse 3, 3010 Bern, Switzerland.
E-mail addresses: malavika.nambiar@unibe.ch (M.H. Nambiar), layko.liechti@unibe.ch (L. Liechti), fabian.mueller@ziemergroup.com (F. Müller), werner.bernau@ziemergroup.com (W. Bernau), harald.studer@optimo-medical.com (H. Studer), asroy27@yahoo.com (A.S. Roy), theo@seiler.tv (T.G. Seiler), Philippe.buechler@unibe.ch (P. Büchler).

https://doi.org/10.1016/j.exer.2022.109266
Received 7 July 2022; Received in revised form 31 August 2022; Accepted 20 September 2022
Available online 27 September 2022

Wollensak et al., 2003), which is the most popular test. However, the biomechanical characterization of porcine corneas showed important variations in the stress-strain relationship. For example, the results of uniaxial tests vary widely among published studies, with values for stress at 10% strain ranging from 0.12 MPa to 1.8 MPa in full-thickness corneal strips evaluated in the superior-inferior direction at low strain rates ranging from 0.005%/s – 0.16%/s (Boschetti et al., 2012; Elsheikh et al., 2008, 2011; Kampmeier et al., 2000; Wollensak et al., 2003). One of the factors that may explain this variability is the methods used to calculate the stress in the samples: The cross-section of the samples is difficult to quantify accurately and varies across the sample, with corneal cross-section being larger at the periphery than in the central part of the cornea. As a result, the stress values reported in these studies are questionable and may explain the large variability in the results.

While several studies investigated the effect of specimen orientation on the biomechanics (Boschetti et al., 2012; Du et al., 2017; Elsheikh et al., 2008a; Kampmeier et al., 2000), to our knowledge, there is only one study quantifying the depth dependence of the biomechanical response of the porcine cornea (Du et al., 2017). This study found no difference in nasal-temporal (NT), superior-inferior (SI) or diagonal directions, but a decreasing stiffness over depth, with the anterior segment being approximately three times stiffer than the posterior one. However, this study measures not only the mechanical response of the stroma but also includes the Bowman's membrane in the anterior region and, the Descemet's membrane and the endothelial layer in the posterior region, which likely influences the measured force and stress. However, they rightly highlight the need for depth-dependent analysis of porcine cornea to truly capture its biomechanical properties.

Only a few anisotropic mechanical models of the porcine cornea have been derived from such experimental studies (Cornaggia et al., 2020; Elsheikh et al., 2011; Pandolfi and Boschetti, 2015). While many numerical models exist for the human cornea, numerical modeling of the porcine cornea is scarce. The few porcine models available in the literature describe the stroma with the same collagen fiber arrangement as in humans with two orthogonal fiber families (Cornaggia et al., 2020; Elsheikh et al., 2011; Pandolfi and Boschetti, 2015). This modeling approach contradicts the circular arrangement of a single family of collagen in porcine corneas observed in X-ray diffraction analyzes (Hayes et al., 2007).

Therefore, this study aims to characterize the mechanical properties of porcine stroma at different orientations and depths, and to determine the mechanical parameters of a nonlinear, anisotropic mechanical model. To control sample preparation, strips were cut with a femtosecond laser to ensure uniform geometry and thickness and for a precise control of sample depth. Uniaxial tests were performed with hook attachment of the samples to avoid squeezing the tissue at the attachment and to allow a more natural contraction of the specimen in the plane orthogonal to the tensile force. In addition, we used inverse finite element modelling to determine the mechanical properties of the constitutive models of the cornea, taking into account the size of the specimen, the experimental attachment, as well as the actual change in shape of the sample during experimental testing.

2. Materials and methods

2.1. Experimental set up

Forty fresh porcine eyes aged 3–4 months were obtained from the local slaughterhouse. Each eye was randomly assigned to one of three groups: NT, SI, or diagonal. The diagonal direction could be at $+45^{\circ}$ or -45° from the horizontal axis. The entire eyeball was placed in an in-house built pressurization device with the cornea facing upward to prevent movement during strip cutting with the Femto LDV Z8 Ziemer femtosecond laser (Ziemer Ophthalmic Systems AG, Switzerland). Two drops of 0.5% hyaluronic acid were administered on the cornea and then rinsed with water. The laser handpiece was then centered on the cornea using the OCT integrated in the Femto LDV Z8 device. The OCT was also used to ensure that the total corneal thickness remained greater than 750 μm to avoid perforations, thinner corneas were excluded from the study. For each eye, three strips 8 mm long and 3.5 mm wide were cut in the desired corneal orientations. These strips were cut at depths of alternating 100 μm and 150 μm. In this way, samples with a thickness of 150 μm were obtained at a depth of 100 μm (D1), 350 μm (D2) and 600 μm (D3) in NT, SI, and diagonal directions, measured from the top surface of the strip. They were individually preserved and tested in a hydration preserving culture media containing 5% Dextran (Fig. 1) (Hamon et al., 2021).

The strips were uniaxially tested in less than 10 h after collection in a bath containing the same culture media using the Ustretch device (CellScale, Waterloo, Canada), at room temperature. The tissue was pre-stretched with a small force of 20 mN to ensure uniform tension across the samples. The samples were then loaded with 6 cycles at a strain rate of 0.75%/s. The last cycle of force displacement data was recorded for analysis; as the mechanical response of the tissue stabilized after the fifth cycle of preconditioning. The strain rate was chosen after a preliminary study showing only marginal changes in the force/displacement relationship up to a rate of 0.75%/s, which allows to minimize viscous effect while limiting the test duration. The specimens were tested up to a strain of 13%, which is consistent with previous experiments (Boschetti et al., 2012; Elsheikh et al., 2008, 2011; Wollensak et al., 2003). The force displacement data was used for numerical modelling and statistical analysis. To calculate the strain the true length of the sample was considered: The distance between the grips was 5.5 mm, but this distance increases under the pre-stretch 20 mN because of the effects of both the tensioning of the testing device and the deformation of the sample. To distinguish the two effects and calculate the strain in the sample, the reference length of the sample was calculated using the slope of the force-displacement curve at 20 mN and extrapolating it to determine the length corresponding to a force of 0 mN (Fig. 2). The strain was then calculated as the ratio of extension to this reference length of the sample.

2.2. Statistical methods

Statistical analysis was performed using a mixed model effect on RStudio (RStudio Team, 2022), with depth and orientation as the fixed parameters, samples as a random variable, and the measured force as the dependent variable. A one-way ANOVA was performed on each depth group to analyze the difference between orientations.

2.3. Finite element model

The finite element model has the same geometry and boundary conditions as the experimental setup (Fig. 3). The hook attachment points were modelled as three holes with a diameter of 0.25 mm and

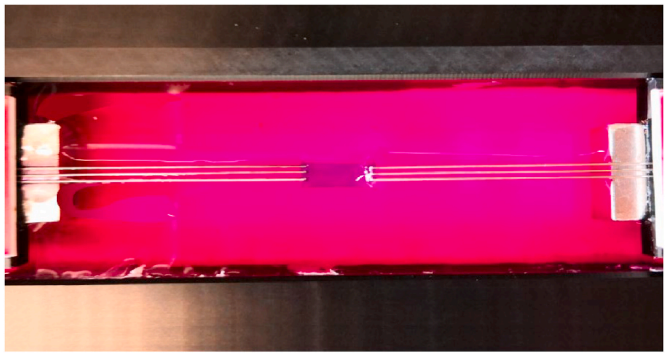

Fig. 1. The strips were tested under traction in a bath of MEM + 5% Dextran using BioRake attachments.

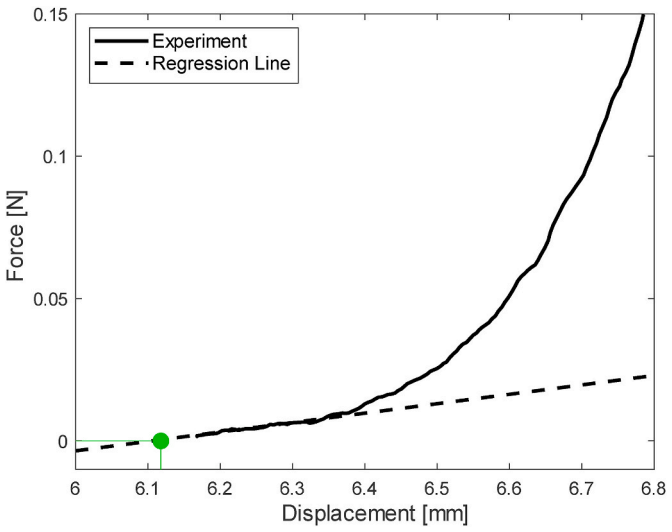

Fig. 2. The reference length of the specimen was determined by extrapolating the tangent to the force-displacement measurement to zero force.

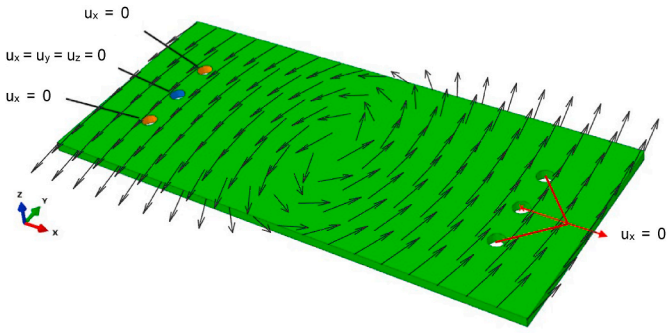

Fig. 3. Finite element model of the strip used to determine its mechanical properties. It shows the boundary conditions applied to the model and an example of the distribution of the main direction of anisotropy.

with a distance of 0.7 mm between their centers. Boundary conditions were applied to the attachment holes: The model was fixed on one side, while a displacement was imposed on the opposite side. On the fixed side, the central hole was encastered, and the outer holes were fixed only in the direction of traction. On the moving side, the surface of the holes was coupled to a reference point to which the experimentally measured displacement was applied, while allowing for lateral contraction (Fig. 3). The model was meshed with approximately 600 s-order hexahedral elements.

The mechanical behavior of the stroma was described using two nonlinear, hyperelastic, incompressible constitutive models. To account for the different dispersion of collagen fibers in the plane of the cornea and out of this plane, the general structure tensor proposed by Holzapfel et al. (Gasser et al., 2006; Holzapfel et al., 2000) was used (1). As the material was assumed incompressible, the deformation was described using invariants of the isochoric Cauchy green strain tensor $\overline{\mathbf{C}} = \boldsymbol{J}^{2/3}\mathbf{F}^{T}\mathbf{F}$, where **F**is the deformation gradient tensor and $J = det\ \mathbf{F}$ is the volumetric ratio. The strain-energy function describing the mechanical behavior is based on the strain invariants $\overline{I}_1$ and $\overline{I}_4$, defined as follows:

$$\overline{I}_1 = Tr\,\overline{\mathbf{C}}$$
$$\overline{I}_4 = (\mathbf{H}\otimes\mathbf{H}) : \overline{\mathbf{C}}$$

$$\mathbf{H} = 2\kappa_o\kappa_i\mathbf{I} + 2\kappa_o(1-2\kappa_i)(M\otimes M) + (1-2\kappa_o-2\kappa_o\kappa_i)(M_{\mathbf{n}}\otimes M_{\mathbf{n}}) \quad (1)$$

Where M is a vector describing the mean fiber direction and M_n is the out-of-plane direction. The parameters $\kappa_i \in [0,1]$ and $\kappa_o \in [0, 1/2]$quantify the in-plane and out-of-plane fiber dispersion.

The material behavior was described using the anisotropic model of Gasser, Holzapfel, and Ogden (Gasser et al., 2015; Holzapfel et al., 2000) (2), and the model proposed by Markert et al. (2005) (3). These two models have been chosen because they are frequently used to model the cornea (Ariza-Gracia et al., 2017; Pandolfi and Manganiello, 2006; Studer et al., 2010, 2013; Wang and Hatami-Marbini, 2021; Whitford et al., 2015, 2018).

$$U = C_{10}(\overline{I}_1 - 3) + \frac{k_1}{2k_2}\left\{\exp\left[k_2(\overline{I}_4 - 1)^2\right] - 1\right\} \quad (2)$$

$$U = C_{10}(\overline{I}_1 - 3) + \frac{\mu}{\gamma}\left(\overline{I}_4^{\gamma/2} - 1\right) - \mu \ln \overline{I}_4^{1/2} \quad (3)$$

where C_{10}, k_1, k_2, μ and γ are material parameters and U is the strain energy. Collagen fibers were modelled with a circular orientation. Both material models were implemented in a user-defined subroutine (UMAT) in the commercial finite element solver ABAQUS (Dassault Systemes Simulia Corp, 2020).

An inverse finite element approach was used to determine the material parameters using the force displacement data. In both models, the in-plane fiber dispersion parameter, κ_i was set to 0.454 based on the X-ray scattering data of Hayes et al. (2007). This calculation was performed by taking the integral of the normal distribution that best fit the X-ray scatter intensity. The other material parameters were obtained by simultaneously fitting the numerical model to the average force-displacement of the 9 sets of experimental data, corresponding to the three depths and three orientations. The parameters k_1 and μ were assumed to be different for the deeper layer D3, resulting in a total of 5 parameters for each model: C_{10}, $k_{1,d12}$, $k_{1,d3}$, k_2, κ_o for the HGO model, and C_{10}, μ_{d12}, μ_{d3}, γ, κ_o for the Markert model. A Bayesian optimization process was used to identify the material parameters that best fit the experimental data using the average root mean squared distance between the numerical and experimental data as the loss function.

To validate the determined material parameters, a finite element model was created to reproduce inflation tests from the literature (Elsheikh et al., 2008b). Due to the lack of specific geometry data, the geometry of an average porcine cornea was chosen for the numerical model (Menduni et al., 2018). The inflation model was constructed with depth dependence to remain consistent with the identified material models. For this purpose, the posterior third of the cornea was assigned $k1_{d3}$ and μ_{d3} to the Holzapfel and Markert models, respectively, and all other parameters were set constant for all layers. The model was fixed at the limbus to represent experimental conditions and meshed with approximately 60,000 quadratic tetrahedral elements. Apical displacement was plotted as a function of posterior pressure up to 160 mmHg for comparison with experimental data.

3. Results

120 strips were cut from the 40 porcine eyes. Thirty-four of the strips were excluded from the analysis, bringing the total number of samples for all groups to 86. The main reason for exclusion was damage to the sample – usually around the attachment – or loosening at the attachment points. At least eight samples were available in each group (Table 1).

The force-displacement response under uniaxial measurement was

Table 1
Number of samples tested in each depth and orientation.

	D1	D2	D3	Total
NT	8	9	9	26
SI	8	11	12	31
Diagonal	9	11	9	29
Total	25	31	30	86

determined for the three orientations at different depths. Besides the typical nonlinear force-displacement relationship, our results showed that the properties of the stroma remain constant in D1 and D2 but decrease in the most posterior stromal layer D3. At 12% strain, D1 and D3 show a significant difference ($p < 0.001$), as do D2 and D3 ($p < 0.001$). Moreover, the properties in D1 and D2 were similar across the different orientation ($p = 0.504$), but the SI direction showed higher force than the other directions in the posterior layer D3 ($p < 0.0001$ and $p = 0.049$ when compared to diagonal and NT, respectively) (Fig. 4).

The force was also evaluated at different strain levels (Table 2). As the strain increases, there is a trend for the difference in force between D1-D2 groups to decrease, while always being significantly higher for groups D1 and D2 than D3 ($p < 0.001$). This trend was opposite for the effect of the strip orientation on the force: The differences in measured force for the different orientations increases with strain.

After optimization of the mechanical parameters, both the HGO and Markert models showed good agreement with the experimental data (Fig. 5). The parameters obtained for the models are listed in Table 3. Both models provided a similar value below 50 kPa for C_{10}, which characterizes the part of the models that describes the matrix. Equally interesting was the agreement in depth dependence in the D3 group, where the linear part of the fiber contribution for both models (k1 and μ1 for the HGO and Markert models, respectively) was approximately divided by two for the posterior cornea D3 compared with the anterior layers D1 and D2. While the in-plane dispersion of the fibers was set to a value of 0.45 based on the X-ray diffraction data of Hayes et al. (2007), the value of the out-of-plane dispersion was optimized and both models resulted in a value of approximately 0.37. This value corresponds to a fairly strong in-plane alignment. Although the values appear similar, the distribution corresponding to each of these values is quite different (Fig. 6d). The main fiber direction follows a circular alignment around the direction of the visual axis. Defining a local coordinate system in which the x-axis is defined by the fiber orientation and the y-axis points to the center of the cornea and the z-axis perpendicular to the corneal surface (Fig. 6c), our results show that the fibers are more aligned (lower dispersion) in the plane perpendicular to the fiber curvature (x-z) than in the plane perpendicular to the cornea (x-y) (Fig. 6a & b). Mechanically, this means that the fibers are approximately organized in layers of relatively isotropic fibers across the corneal thickness, with alignment along the x-axis predominating.

The inflation model developed to validate the material models showed good agreement between the simulation with the identified parameters and the experiments for the HGO model. However, the Markert material model could not reproduce the experimental results (Fig. 7).

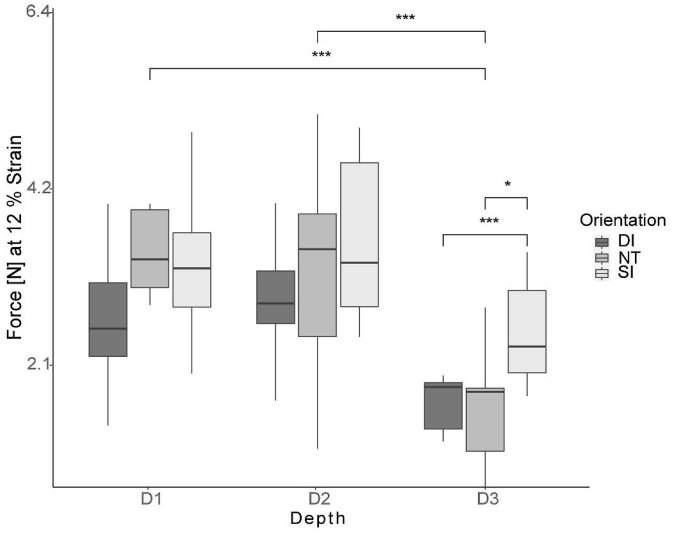

Fig. 4. Force (N) reported at 12% strain across the three depths (D1, D2 and D3) and three orientations (SI, NT and Diagonal) with significant differences indicated.

4. Discussion

The objective of this study was to develop a numerical model of the porcine cornea based on experimental uniaxial test data obtained across the depth of the porcine stroma. The biomechanics of porcine corneas was quantified by uniaxial testing at three depths and in three directions. These experimental data were used to determine the parameters of two nonlinear, anisotropic mechanical models. Our results showed lower stiffness in the posterior part of the cornea. Moreover, the mechanical behaviour of porcine cornea was essentially independent of its orientation in the anterior layers. Only the most posterior layer showed a dependence on orientation with a stiffer response in the SI direction compared with the DI and NT directions. Our experimental and numerical results support the idea of a circumferential orientation of the collagen in the anterior part of the cornea, whereas a slightly elliptical alignment towards the SI direction applies to the posterior cornea.

Although the porcine cornea is a widely accepted model to replace human tissue for ex vivo testing, its mechanical characterization remains inconsistent. In the existing literature, results differ even on crucial aspects such as the dependence of corneal mechanical response on orientation. Some authors present the SI direction as stiffer than NT (Boschetti et al., 2012; Elsheikh, A. et al., 2008), other studies found no difference between these two orientations but reported higher stiffness for the diagonal direction (Elsheikh and Alhasso, 2009), and some reported the same response for all test directions (Du et al., 2017). One possible explanation for this variability is that porcine corneas show only weak dependence on the orientation of the strip cut radially into the cornea. This hypothesis is consistent with our results, which showed little dependence of mechanical properties on orientation. It should be noted that this does not mean that porcine cornea is an isotropic material, but rather that its anisotropic behavior cannot be captured by the test method used in these studies. In fact, the results of this study are consistent with predominant circular orientation of collagen fibers proposed by Hayes et al. based on X-ray scattering measurements.

To date, little attention has been paid to the depth variation of mechanical properties. To our knowledge, only one study has investigated biomechanical properties using strips manually cut at three depths in porcine corneas (Du et al., 2017). While their results are consistent with our observation of a weaker posterior cornea, they also reported that the foremost layer was approximately twice as stiff as the central cornea. One possible reason for this difference is the different positioning of the samples in the depth of the cornea: Our specimens were located slightly more anteriorly, which could make them less susceptible to having their stiffness reduced by swelling that primarily affects the posterior side of the cornea. In addition, when cutting the strips manually, it is more difficult to precisely control their position and ensure a constant and uniform thickness than when cutting them with a femtosecond laser. In the present study, we took care to include only stromal tissue in the strip by using OCT imaging to determine the position of the strips within the cornea.

Previous experimental studies calculate the stress in the specimen as the measured force divided by the cross-section of the sample rather than relying on inverse finite element simulations. Using this approach with our experimental results, considering a cross-section of 0.15 mm × 1.56 mm (thickness x distance between the rakes), the stresses calculated in this study are within the range of those in the literature (Elsheikh et al., 2011; Elsheikh and Alhasso, 2009; Kampmeier et al., 2000; Wollensak et al., 2003).

In the last two decades, numerical techniques such as finite element analysis have become increasingly popular to study corneal diseases or predict the outcome of surgical techniques (Nejad et al., 2014; Studer

Table 2
Statistical comparison of the stress measured for samples at different depth and orientations, reported for different level of stain.

Groups	p-value							
	6% strain		8% strain		10% strain		12% strain	
D1-D2	0.004	**	0.047	*	0.440		0.504	
D2-D3	<0.001	***	<0.001	***	<0.001	***	<0.001	***
D1-D3	<0.001	***	<0.001	***	<0.001	***	<0.001	***
SI- NT	0.786		0.387		0.001	**	0.049	*
NT- Diagonal	0.131		0.074		0.161		0.081	
SI – Diagonal	0.064		0.006	**	0.073		0.002	***

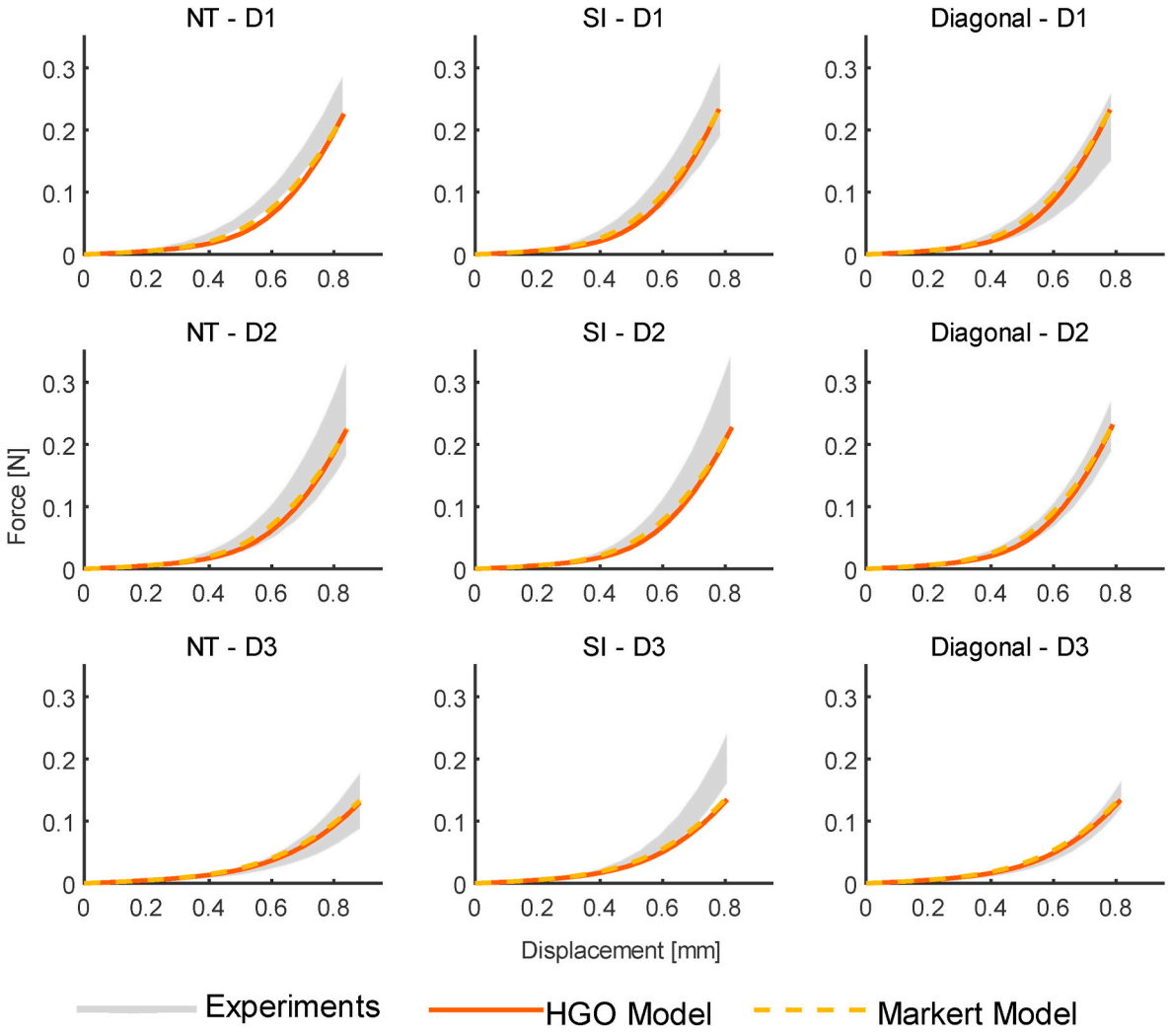

Fig. 5. Force-displacement relationship for the three different orientations (columns) and three depths (rows). The shaded area represents the experimental data (mean ± sd). The result of the numerical optimization is shown for the HGO (red) and Markert models (yellow). (For interpretation of the references to colour in this figure legend, the reader is referred to the Web version of this article.)

Table 3
Parameters of the two material models identified using the experimental data.

	C10 (MPa)	$k1_{d1,2}$ (MPa)	$k1_{d3}$ (MPa)	k2 (−)	$\mu_{d1,2}$(MPa)	μ_{d3}(MPa)	γ(−)	κ_i	κ_o
HGO	0.046	103.5	57	149.5	–	–	–	0.45	0.37
Markert	0.046	–	–	–	11.4	6.5	33.7	0.45	0.36

et al., 2010, 2013). However, little attention has been paid to numerical modeling of porcine corneas. The few numerical studies assume a collagen arrangement identical to that of human tissue based on two orthogonal fiber families (Cornaggia et al., 2020; Pandolfi and Boschetti, 2015). Both authors justified their choice by the lack of data, despite the circular arrangement observed by X-ray diffraction. In contrast, the

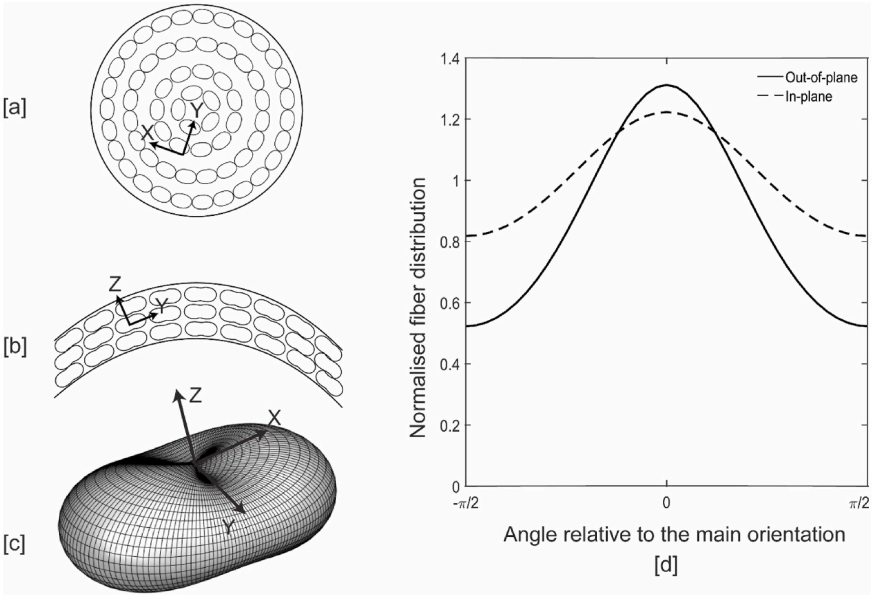

Fig. 6. Graphical representation of [a] in-plane ($\kappa_i = 0.45$) and [b] out-of-plane ($\kappa_o = 0.37$) dispersion on the contour of a cornea as seen from the top view and front view respectively, [c] 3D view of the dispersion. [d] The probability distribution of the $\kappa_i$and $\kappa_o$fiber dispersion along the direction of fiber alignment.

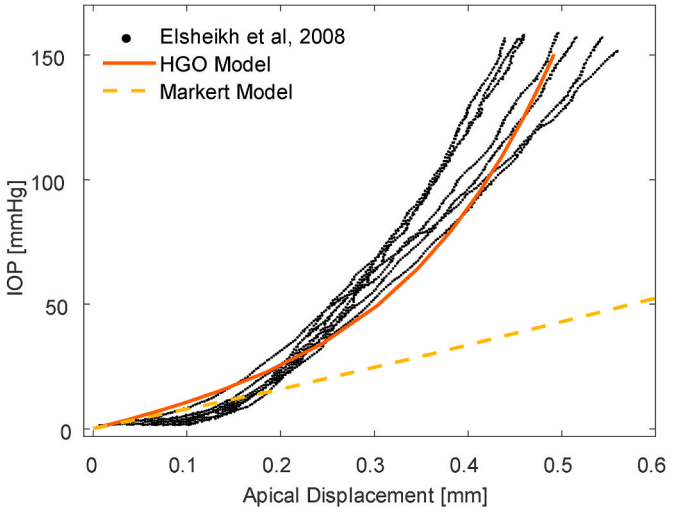

Fig. 7. Comparison of the numerical model identified in this study with experimental inflation data(Elsheikh et al., 2008b). The experimentally determined IOP as a function of apical displacement (black) is compared with the numerical simulation performed with the depth- and orientation-dependent mechanical properties determined in this study for the HGO (Holzapfel et al., 2000) (red) and Markert (Markert et al., 2005) (yellow) models. (For interpretation of the references to colour in this figure legend, the reader is referred to the Web version of this article.)

numerical model in this study, assumes a circular collagen alignment. To the best of our knowledge, this is the first numerical study to use a fiber alignment that is compatible with both, x-ray diffraction measurements (Hayes et al., 2007) and experimental data collected on strips tested in different orientations. This difference in collagen arrangement and the fact that previous studies considered the same in-plane and out-of-plane fiber distribution prevent a direct comparison of the parameter values of the mechanical models with similar models in the literature (Elsheikh et al., 2011).

Unlike human tissue, imaging data are lacking to understand the depth dependence of fiber dispersion in porcine corneas. Therefore, it is difficult to attribute the change in mechanical response to a specific microstructural component: It may be due to either a change in fiber dispersion or fiber density with depth. This study considers only the depth-dependent fiber density and to exclude the depth variation from the parameter identification in order to minimize the number of parameters to be identified and thus to avoid local minima in the optimization procedure.

Using the depth-dependent HGO parameters obtained in this study, we modelled an average porcine cornea under inflation loading and found that the numerical model showed good agreement with published experimental data (Elsheikh et al., 2008b) (Fig. 7). This result confirms the validity of the mechanical description of the cornea using the HGO model and the parameters determined in this study. However, the Markert model obtained in this study could not reproduce the inflation experiment (Fig. 7). This suggests that additional experimental testing is needed to calibrate this model under typical loading conditions such as biaxial or shear. Additional load cases could also help improve the HGO model, which seems to slightly overestimate the stress reported at the low strain of the inflation test.

In contrast to isotropic materials, the stress-strain relationship derived from uniaxial testing of anisotropic materials is likely to depend on the dimensions of the test specimen. In particular, the circular arrangement of collagen fibers in porcine corneas leads to different mechanical responses as a function of specimen length and width: strips with a larger width-to-length ratio recruit more fibers in tension than strips with smaller dimensions. Even when considering a purely uniaxial test condition using finite element simulations based on the identified HGO material model, the size of the specimen leads to important variations in the first Piola-Kirchoff stress calculated as the tensile force divided by the undeformed cross-section of the sample, which is consistent with the calculation of stress from experimental data in the literature (Fig. 8). The fact that the relationship between stress and strain depends on the dimensions of the tested specimen has not been previously considered and means that numerical modeling and inverse parameter identification are required to properly characterize the mechanical response of this fiber-reinforced material. Inverse parameter identification based on finite element simulation offers a unique advantage: since this approach takes into account the actual testing environment, it is not affected by varying cross-section of the specimen, its aspect ratio (which affects the mechanical simulation in the case of anisotropic material), or boundary conditions.

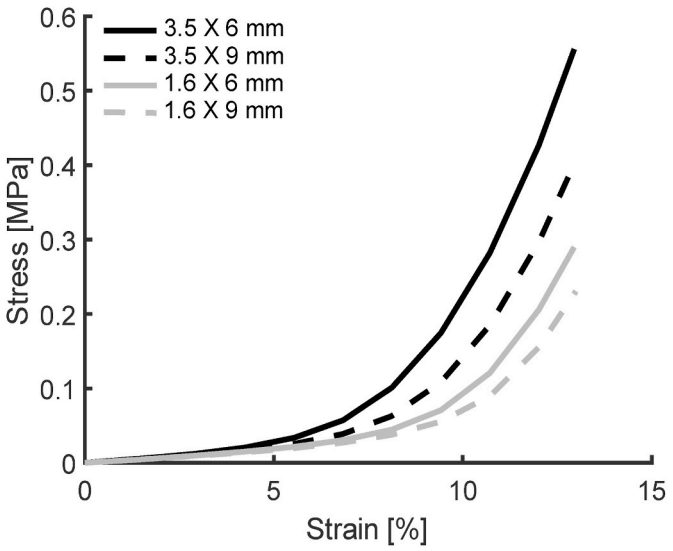

Fig. 8. Stress [MPa] and Strain [%] of a pure uniaxial analysis using the developed material model tested on different dimension configurations seen as 'width X length (mm)', illustrating highest stress for the largest width to length ratio.

While the in-plane dispersion of the fibers was determined by the X-ray scattering data allowing this parameter to be fixed during optimization, the out-of-plane dispersion could not be quantified from that study and was therefore included in the optimization process. Overall, both in-plane and out-of-plane dispersion showed a contribution from isotropic fibers. Nevertheless, it is interesting to observe that the resulting out-of-plane dispersion corresponds to fibers approximately following the curvature of the cornea, while the in-plane dispersion represents a circular alignment of fibers in the plane of the cornea with a stronger isotropic contribution (Fig. 6). These results also showed the importance of considering both dispersions, rather than assuming a completely symmetry dispersion of fibers about the main direction of anisotropy. The important isotropic fiber dispersion also means that the fibers make a relevant contribution to the force measured in this uniaxial measurement, even if the predominantly circular fiber direction is perpendicular to the test direction. In fact, Hayes et al. classified a significant portion of the diffraction signal as isotropic scattering from corneal collagen, which provides a mechanical response for all test directions and suggests that our test method may be testing the more randomly oriented collagen fibers of the cornea. Circumferential samples taken from the periphery of the cornea could provide more information on the effects of fiber orientation on the mechanical response.

Despite the promising results, we are aware of the limitations of this study. The first 100 μm of the cornea are discarded in the testing protocol because they contain the epithelial layer, which makes no mechanical contribution. Recently, porcine corneas were also found to contain a Bowman membrane in this discarded anterior layer (Hammond et al., 2020). However, it has been reported that the Bowman membrane in humans has only a marginal effect on the mechanical response of the stroma (Kling et al., 2020; Torres-Netto et al., 2021), and because the thickness of the Bowman membrane in pigs is about 10 times thinner, we can assume that its mechanical contribution in pig corneas is also negligible. Therefore, it can be assumed that the tissue of the anterior layer that was discarded does not make a relevant mechanical contribution, and it is therefore acceptable to focus the material characterization on the corneal stroma. Another limitation relates to the sample depth: the three test depths were taken at a fixed distance from the anterior cornea in all eyes. Although little swelling was observed in our specimen, the testing depth does not correspond to the same proportion of corneal thickness in all samples. However, preparation of the sample with a femtosecond laser guarantees uniform thickness of the strips, and precise selection of their depth and orientation, ensuring reproducibility of measurements and quality of parameter identification.

The strain rate of 0.75%/s used in this study is higher than the low strain rate commonly used in the literature (0.13%/s – 0.16%/s) (Elsheikh et al., 2011; Kampmeier et al., 2000; Wollensak et al., 2003). However, we did not observe any difference in the mechanical response after preconditioning the strips, which were tested at strain rates of 0.16%/s, 0.75%/s, and 1.5%/s. Therefore, in the interest of time, a strain rate of 0.75%/s was chosen for these experiments. Another important difference from existing studies is the use of BioRake (CellScale, Waterloo, Canada) attachments instead of clamps. This method is closer to uniaxial loading because it avoids squeezing the cornea at the attachment and allows some lateral contraction of the specimen. This aspect is even more critical in this study because the attachment is to a thin stromal layer rather than the entire stroma. In addition, finite element modeling was used to identify the mechanical parameters from the force-displacement measurements. Since these models take into account the actual boundary conditions acting on the specimen and its progressive deformation during the measurement, these effects have less influence on the identified parameters than simply approximating the stress as the ratio between the force and the cross-section of the sample at the beginning of the measurement.

5. Conclusion

This study proposed a model of the porcine cornea based on an anisotropic and inhomogeneous mechanical model. Our mechanical results confirmed imaging data showing that the porcine cornea is a transversely isotropic material in which the fibers are predominantly oriented in a circular direction. Moreover, the mechanical properties of the stroma remain constant up to the middle of the cornea and then decrease posteriorly. The parameters of an identified HGO model were also able to reproduce corneal inflation, suggesting that it is suitable for simulating the mechanical response of the entire cornea. Our results also indicate that caution should be exercised when testing anisotropic soft tissues because the size of the specimen affects the stress calculated as the ratio of force to cross-section, which means that numerical models are needed to compare the results of different experimental studies. Such a model constitutes the basis for in silico platforms to develop new ophthalmic treatments. In this way, researchers can match their experimental surrogate porcine model with a numerical counterpart and validate the prediction of their algorithms in a complete and accessible environment.

Funding

This study was funded by the SNSF grant (No. IZLIZ3_182975). There are no conflicts of interests.

Data availability

Data will be made available on request.

References

Ahearne, M., Yang, Y., Then, K.Y., Liu, K.K., 2007. An indentation technique to characterize the mechanical and viscoelastic properties of human and porcine corneas. Ann. Biomed. Eng. 35, 1608–1616. https://doi.org/10.1007/s10439-007-9323-9.

Ariza-Gracia, M., Ortillés Cristóbal, J., Rodríguez Matas, J.F., Calvo, B., 2017. A numerical-experimental protocol to characterize corneal tissue with an application to predict astigmatic keratotomy surgery. J. Mech. Behav. Biomed. Mater. 74, 304–314. https://doi.org/10.1016/j.jmbbm.2017.06.017.

Bekesi, N., Dorronsoro, C., De La Hoz, A., Marcos, S., 2016. Material properties from air puff corneal deformation by numerical simulations on model corneas. PLoS One 11. https://doi.org/10.1371/journal.pone.0165669.

Boschetti, F., Triacca, V., Spinelli, L., Pandolfi, A., 2012. Mechanical characterization of porcine corneas. J. Biomech. Eng. 134, 1–9. https://doi.org/10.1115/1.4006089.
Carter, R.B., 1872. Lectures on operative opthalmic surgery. Lancet 1–3.
Cornaggia, A., Boschetti, F., Mazzotta, C., Pandolfi, A., 2020. Numerical investigation on epi-off crosslinking effects on porcine corneas. Mech. Soft Mater. 2 https://doi.org/10.1007/s42558-020-00030-7.
Du, R., Tian, H., Xu, X., Shao, Y., Song, F., 2017. Depth-dependent mechanical characteristics of porcine cornea. Soft Mater. 15, 27–33. https://doi.org/10.1080/1539445X.2016.1242497.
Elsheikh, A., Brown, M., Alhasso, D., Rama, P., Campanelli, M., Garway-Heath, D., 2008a. Experimental assessment of corneal anisotropy. J. Refract. Surg. Off. Publ. Int. Soc. Refract. Surg. 24.
Elsheikh, A., Alhasso, D., 2009. Mechanical anisotropy of porcine cornea and correlation with stromal microstructure. Exp. Eye Res. 88, 1084–1091. https://doi.org/10.1016/j.exer.2009.01.010.
Elsheikh, A., Alhasso, D., Rama, P., 2008b. Biomechanical properties of human and porcine corneas. Exp. Eye Res. 86, 783–790. https://doi.org/10.1016/j.exer.2008.02.006.
Elsheikh, A., Kassem, W., Jones, S.W., 2011. Strain-rate sensitivity of porcine and ovine corneas. Acta Bioeng. Biomech. 13.
Gasser, T.C., Ogden, R.W., Holzapfel, G.A., 2015. Modelling non-symmetric collagen fibre dispersion in arterial walls. J. R. Soc. Interface 3, 15–35. https://doi.org/10.1098/rsif.2005.0073.
Gasser, T.C., Ogden, R.W., Holzapfel, G.A., 2006. Hyperelastic modelling of arterial layers with distributed collagen fibre orientations. J. R. Soc. Interface 3, 15–35. https://doi.org/10.1098/rsif.2005.0073.
Hammond, G.M., Young, R.D., Muir, D.D., Quantock, A.J., 2020. The microanatomy of Bowman's layer in the cornea of the pig: changes in collagen fibril architecture at the corneoscleral limbus. Eur. J. Anat. 24, 399–406.
Hamon, L., Daas, L., Mäurer, S., Weinstein, I., Quintin, A., Schulz, K., Langenbucher, A., Seitz, B., 2021. Thickness and curvature changes of human corneal grafts in dextran-containing organ culture medium before keratoplasty. Cornea 40, 733–740. https://doi.org/10.1097/ICO.0000000000002543.
Hatami-marbini, H., 2014. Viscoelastic shear properties of the corneal stroma. J. Biomech. 47, 723–728. https://doi.org/10.1016/j.jbiomech.2013.11.019.
Hayes, S., Boote, C., Lewis, J., Sheppard, J., Abahussin, M., Quantock, A.J., Purslow, C., Votruba, M., Meek, K.M., 2007. Comparative study of fibrillar collagen arrangement in the corneas of primates and other mammals. Anat. Rec. 290, 1542–1550. https://doi.org/10.1002/ar.20613.
Holzapfel, G.A., Gasser, T.C., Ogden, R.A.Y.W., 2000. A New Constitutive Framework for Arterial Wall Mechanics and a Comparative Study of Material Models 1–48.
Kampmeier, J., Radt, B., Birngruber, R., Brinkmann, R., 2000. Thermal and biomechanical parameters of porcine cornea. Cornea 19, 355–363. https://doi.org/10.1097/00003226-200005000-00020.
Kling, S., Torres-Netto, E.A., Spiru, B., Sekundo, W., Hafezi, F., 2020. Quasi-static optical coherence elastography to characterize human corneal biomechanical properties. Investig. Ophthalmol. Vis. Sci. 61, 11–14. https://doi.org/10.1167/IOVS.61.6.29.
Markert, B., Ehlers, W., Karajan, N., 2005. A general polyconvex strain-energy function for fiber-reinforced materials. Pammatone 5, 245–246. https://doi.org/10.1002/pamm.200510099.
Menduni, F., Davies, L.N., Madrid-Costa, D., Fratini, A., Wolffsohn, J.S., 2018. Characterisation of the porcine eyeball as an in-vitro model for dry eye. Contact Lens Anterior Eye 41, 13–17. https://doi.org/10.1016/j.clae.2017.09.003.
Nejad, T.M., Foster, C., Gongal, D., 2014. Finite element modelling of cornea mechanics: a review. Arq. Bras. Oftalmol. 77, 60–65. https://doi.org/10.5935/0004-2749.20140016.
Pandolfi, A., Boschetti, F., 2015. The influence of the geometry of the porcine cornea on the biomechanical response of inflation tests. Comput. Methods Biomech. Biomed. Eng. 18, 64–77. https://doi.org/10.1080/10255842.2013.778983.
Pandolfi, A., Manganiello, F., 2006. A model for the human cornea: constitutive formulation and numerical analysis. Biomech. Model. Mechanobiol. 5, 237–246. https://doi.org/10.1007/s10237-005-0014-x.
Roberts, C.J., 2016. Importance of accurately assessing biomechanics of the cornea. Curr. Opin. Ophthalmol. 27, 285–291. https://doi.org/10.1097/ICU.0000000000000282.
Sanchez, I., Martin, R., Ussa, F., Fernandez-Bueno, I., 2011. The parameters of the porcine eyeball. Graefe's Arch. Clin. Exp. Ophthalmol. 249, 475–482. https://doi.org/10.1007/s00417-011-1617-9.
Søndergaard, A.P., Ivarsen, A., Hjortdal, J., 2013. Corneal resistance to shear force after UVA-riboflavin cross-linking. Investig. Ophthalmol. Vis. Sci. 54, 5059–5069. https://doi.org/10.1167/iovs.12-10710.
Studer, H., Larrea, X., Riedwyl, H., Büchler, P., 2010. Biomechanical model of human cornea based on stromal microstructure. J. Biomech. https://doi.org/10.1016/j.jbiomech.2009.11.021.
Studer, H.P., Riedwyl, H., Amstutz, C.A., Hanson, J.V.M., Büchler, P., 2013. Patient-specific finite-element simulation of the human cornea: a clinical validation study on cataract surgery. J. Biomech. 46, 751–758. https://doi.org/10.1016/j.jbiomech.2012.11.018.
Torres-Netto, E.A., Hafezi, F., Spiru, B., Gilardoni, F., Hafezi, N.L., Gomes, J.A.P., Randleman, J.B., Sekundo, W., Kling, S., 2021. Contribution of Bowman layer to corneal biomechanics. J. Cataract Refract. Surg. 47, 927–932. https://doi.org/10.1097/j.jcrs.0000000000000543.
Vail, D., 1956. Ophthalmic surgery. Am. J. Ophthalmol. 41, 1082–1084. https://doi.org/10.1016/0002-9394(56)91083-2.
Wang, S., Hatami-Marbini, H., 2021. Constitutive modeling of corneal tissue: influence of three-dimensional collagen fiber microstructure. J. Biomech. Eng. 143, 1–9. https://doi.org/10.1115/1.4048401.
Whitford, C., Movchan, N.V., Studer, H., Elsheikh, A., 2018. A viscoelastic anisotropic hyperelastic constitutive model of the human cornea. Biomech. Model. Mechanobiol. 17, 19–29. https://doi.org/10.1007/s10237-017-0942-2.
Whitford, C., Studer, H., Boote, C., Meek, K.M., Elsheikh, A., 2015. Biomechanical model of the human cornea: considering shear stiffness and regional variation of collagen anisotropy and density. J. Mech. Behav. Biomed. Mater. 42, 76–87. https://doi.org/10.1016/j.jmbbm.2014.11.006.
Wollensak, G., Spoerl, E., Seiler, T., 2003. Stress-strain measurements of human and porcine corneas after riboflavin-ultraviolet-A-induced cross-linking. J. Cataract Refract. Surg. 29, 1780–1785. https://doi.org/10.1016/S0886-3350(03)00407-3.
Zeiss, C.J., 2013. Translational models of ocular disease. Vet. Ophthalmol. 16, 15–33. https://doi.org/10.1111/vop.12065.